CONCRETE LIBRARY OF JSCE NO. 33, JUNE 1999

A STUDY ON LIMIT-STATE DESIGN METHOD FOR PRESTRESSED CONCRETE SLEEPERS

(Translation from Proceedings of JSCE, No.557/V-34, February 1997)

Hajime WAKUI

Hiroyuki OKUDA

Prestressed concrete sleepers have gradually been developed over about 50 years. However, with current prestressed concrete sleepers designed by the conventional allowable stress approach, there still remain many problems to be resolved and areas to be improved when viewed from the limit-state design method. The primary hindrance to the rationalization of this type of track component is the fact that dynamic behavior and load carrying capacity under the enormous impact loading of wheels, which is mainly induced by wheel flats, have not yet been thoroughly evaluated. This paper discusses the results of comprehensive investigations into the loading, responses, and resistance of prestressed concrete sleepers aimed at a shift away from the conventional allowable stress design technique to a contemporary design method which involves impulsive wheel loads, dynamic responses, and limit-state behavior.

Keywords: prestressed concrete sleepers, railway track, wheel flats, impact loading, limit-state design, cracking state, fatigue life, impulsive flexural capacity

Hajime WAKUI is General Manager of Ladder Track System Division at Railway Technical Research Institute, Tokyo, Japan. He obtained his D.Eng. from Tokyo Institute of Technology in 1996. His research interests relate to railway vehicle/bridge dynamic interaction. He is a member of JSCE.

Hiroyuki OKUDA is a senior engineer of Ladder Track System Division at Railway Technical Research Institute, Tokyo, Japan. He graduated from Ritsumeikan University in 1976. His research interests relate to dynamic response characteristics in concrete structures. He is a member of JSCE.

1. INTRODUCTION

Prestressed concrete sleepers were first introduced about 50 years ago, and development has continued ever since. Nevertheless, since today's prestressed concrete sleepers (PC sleepers) are an achievement of conventional design based on allowable stress, many problems still remain unsolved when viewed from the new design philosophy that takes account of limit-state behavior, as enumerated below:

1) In the case of Shinkansen (bullet train) lines, in spite of a relatively mild loading environment with well maintained cars and tracks, sleepers are likely to be overdesigned from the viewpoint of design load.

2) For lines in a more severe loading environment, such as heavy freight lines and lines where wheel treads are unsatisfactorily maintained, there is no assurance of adequate load carrying capacity or durability in some cases (Photo 1).

3) Sleeper designs do not amply reflect differences in inherent load carrying capacities of various tensioning techniques, that is, pre-tensioning, bonded post-tensioning, and unbonded post-tensioning.

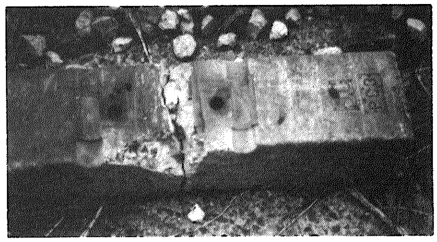

Photo 1 Transverse cracking possibly caused by impulsive loads

Such problems are referred to in a report of the FIP commission on prefabrication [1]. This report points out that the primary factor impeding the rational design of PC sleepers is the fact that not enough knowledge has yet been established on the dynamic behavior and load carrying capacity of sleepers experiencing impulsive wheel loading.

Wheel load variations caused by defects in tracks and cars can be classified into two major categories. One is "quasi-static wheel loading" (comprising static wheel load + variations) mainly generated by vibrations of the car sprung mass (car body mass, etc.) attributable to "usual defects" (ordinary track irregularities, minor irregularities in wheel treads and railheads within control limits, etc.). The other is "impact wheel loading" (comprising load spikes alone, ignoring the static wheel load) mainly set up by collisions between the car unsprung mass (wheel-set mass, etc.) and the track, when there are unusual defects (irregularities in wheel treads and railheads exceeding control limits, floating sleepers, etc.). The discussion in this paper definitely identifies these two kinds of very different wheel loads.

Typical causes of extremely high impact wheel loads are, in the case of continuously welded rail sections, bad welds, railhead corrugations (Photo 2), unusual spots such as floating sleepers, and wheel flats (Photo 3), viz., defective wheel treads caused by wheel locking or skidding. It is reported that wheel flats are particularly likely to cause extremely high impact loads on PC sleepers [2-5], and damage incidences are cited in many reports. This paper deals with wheel flats as the main cause of impact wheel loading.

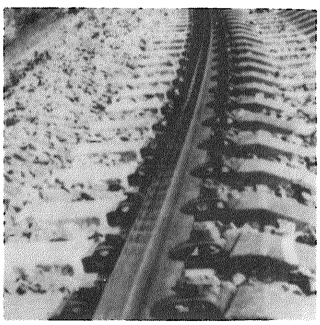

Photo 2 Example of railhead corrugation

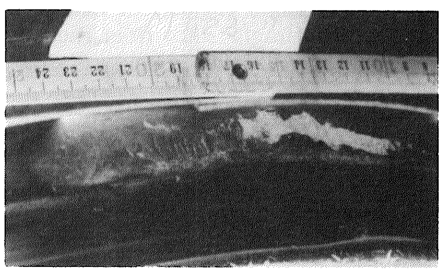

Photo 3 Example of wheel flat

On the basis of the considerations above, the present paper discusses a series of investigations into impulsive loading, structural response, and load carrying capacity, aiming at shifting from the conventional design technique involving "quasi-static wheel load + static response + allowable stress" to a new design method factoring in "impact wheel load + dynamic response + limit-state behavior".

2. CONVENTIONAL PC SLEEPER DESIGN

(1) Summary of Conventional Design Technique

The conventional design technique [6-9] resorts to the following process, usually based on the calculation model shown in Fig. 1.

1) The rail-seat load R is obtained by this equation.

$$R = P_{st} \cdot (1+i_d) \cdot d_f \qquad \text{(Eq. 1)}$$

where P_{st} = design static wheel load, $1+i_d$ = wheel load impact factor, d_f = wheel load distribution factor (0.5 to 0.6).

2) The ballast reaction is uniformly distributed in the range of *2a* on both sides, with the rail position at the center, the *a* denoting the distance from the rail position to the sleeper end.

3) The ballast reaction at the center is assumed to be the product of the uniformly distributed ballast reaction given in 2) multiplied by the center binding coefficient ψ (Fig.1) (center-portion-free state ψ =0, uniformly supported condition ψ =1).

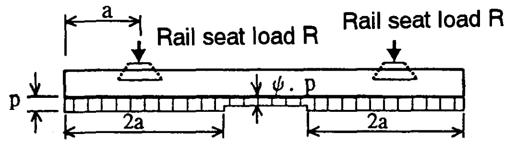

Fig.1 Assumed ballast reactions for computing sleeper flexural moments

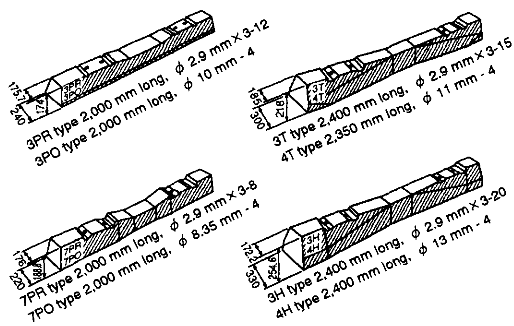

Fig.2 Typical PC sleepers used for JR lines

4) The flexural moments in the sleeper (positive at the rail seat, negative at the center) are statically calculated. Referring to the moments thus obtained,sleepers are so prestressed that they will not crack.

(2) Design Load and Required Load Carrying Capacity by Conventional Design Technique

For typical PC sleepers in different countries mentioned in the report of the FIP Commission on Prefabrication [1] as well as for typical PC sleepers used by JR (Fig.2), the relationship between de-compression moment per unit static wheel load (M_0/P_{st}) and wheel load impact factor ($1+i_d$) is shown in Fig.3. For PC sleepers, since the influence of the dead load can be ignored, the design load can be expressed by the wheel load alone. Figure. 3 also shows the (M_0/P_{st})-to-($1+i_d$) linear relationships resulting from the flexural moment given by the design model in Fig. 1, with a wheel load distribution factor d_f of 0.6 and a center binding coefficient ψ of 0, both for standard gauge sleepers (2,400 mm long) and narrow gauge sleepers (2,000mm long). Figure 3 confirms the following features of the design load and required load carrying capacity as given by the conventional design technique:

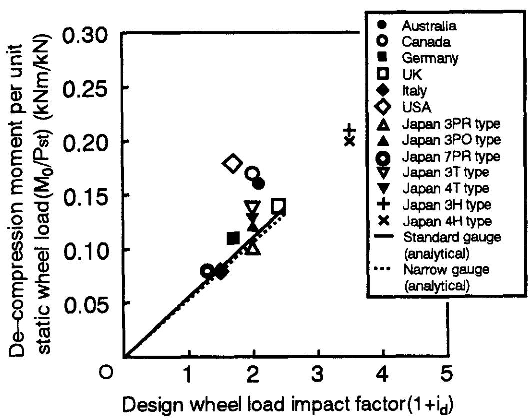

Fig3. Relationship between de-compression moment per unit static wheel load (M_0/P_{st}) and design wheel load impact factor ($1+i_d$) (positive rail-seat flexural moment)

1) The wheel load impact factor ($1+i_d$) ranges widely from 1.3 to 3.5. Most values are, however, 2.5 or less. The conventional design technique basically considers what is called a "quasi-static wheel load" in the present paper.

2) The maximum 3.5 and minimum 1.3 wheel load impact factors ($1+i_d$) are adopted for the PC sleepers

used by JR. The maximum 3.5 relating to 3H and 4H type sleepers is the value determined for Shinkansen high-speed lines, taking into account the extremely high wheel loads experienced in the 1970s with a prototype train dubbed the 951 Type with a heavy unsprung mass [10].

3) The wheel load impact factor ($1+i_d$) which dominates the de-compression moment is completely independent of the differences between pre-tensioned and post-tensioned types.

4) The (M_0/P_{st}) and ($1+i_d$) of each type of PC sleeper generally lies on the (M_0/P_{st})-to-($1+i_d$) linear relationship derived from the design model in Fig. 1.

3. CHARACTERISTICS OF IMPACT WHEEL LOADS DUE TO UNUSUAL DEFECTS

To grasp the characteristics of impact wheel loads induced by unusual defects, the axle-box acceleration of a wheel-set axle-box was measured by mounting an accelerometer in the position shown in Photo 4. This allowed continuous observation from the vehicle side. The axle-box acceleration is deemed representative of the wheel-set acceleration.

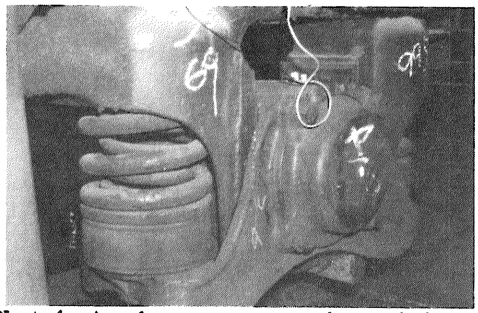

Photo4 Accelerometer mounted on axle-box of wheel-set

(1)Axle-box Acceleration due to Railhead Corrugation

On a section of Shinkansen line with well developed random corrugations caused by corrosion in a submarine tunnel (slab track with 60 kg rail), the axle-box acceleration was measured just before rail renewal. The recorded axle-box acceleration is shown in Fig.4, and the waveform detail at the peak axle-box acceleration, 54.3g, in Fig. 5. A total of 716 shock pulse peaks as well as their duration were picked up from Fig.4. The distribution of peaks and their duration is plotted in Fig. 6. The results of these measurements and analysis demonstrate the following:

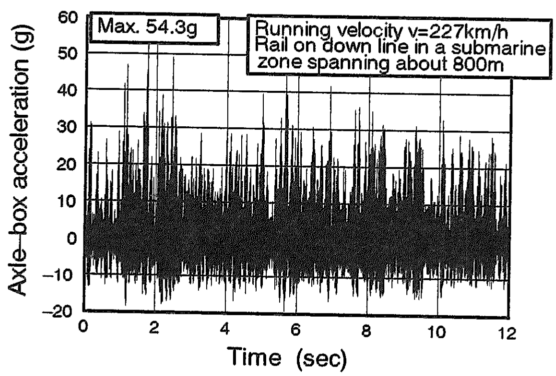

Fig.4 Example of waveform of axle-box acceleration (railhead corrugation)

1) Figure 5 indicates that a negative acceleration of about -10g is recorded just before a shock pulse. This means that, after the wheel tread leave the railhead, it strikes the track under the action of a force built up in the axle spring under the sprung mass weight. Consequently, the impact wheel load acts in the form of load spike.

2) Figure 6 clarifies that dominant shock pulses with peaks exceeding 30g are concentrated in the duration range from 5 to 10 msec (msec = 1/1000 second).

(2) Axle-box Acceleration due to Wheel Flat

An extreme wheel flat (a flat spot 75mm long and about 3 mm deep) was artificially made on a Saha 100 series test car. This electric vehicle ran over the Yamanote line (a commuter loop in Tokyo) with ballasted track (60 kg rail, 3PR and 3PO type sleepers) at speeds of 10 to 85 km/hr to measure the axle-box acceleration. Typical recorded axle-box accelerations are shown in Fig. 7. From this record, as in the case of (1) above, 3591 combinations of shock pulse peaks with their duration were taken. The distribution of the data is shown in Fig.8. The results of these measurements and analysis offer the following knowledge:

1) The maximum axle-box acceleration was 51g.

2) Figure 8 shows that dominant load spikes with peaks exceeding 30g are concentrated in the duration range from 1 to 6 msec.

3) The duration of load spikes clearly tends to decrease with increasing running speed (though no graph is not provided here); that is to say, 5 to 6 msec at 10 km/hr, 2 to 3 msec at 60 km/hr, and 1 msec order at 85 km/h.

(3) Discussion on Characteristics of Impact Wheel Load

From analysis of the axle-box acceleration, the characteristics of impact wheel loading can be summarized as follows:

1) The impact wheel load can be simplified as a shock pulse acting after the static wheel load is removed.

2) The maximum peak value of the shock pulses was 54g (for railhead corrugations) and 51g (for a wheelflat). If a rigid axle is assumed, and the unsprung effective mass is 800 kg / wheel, an axle-box acceleration of 50g corresponds to an impact wheel load of 400 kN. This relationship is, however, only approximate.

3) The duration of dominant shock pulses with peak values exceeding 30g lies between 5 and 10 msec (for railhead corrugations) and 1 to 6 msec (for a wheel flat). It should therefore be taken into account that the duration of impact wheel loading ranges widely, from 1 to 10 msec.

As discussed above, knowledge of impact wheel loading is still just an assembly of information and it is not well systematized. Another problem to be tackled is to determine the correlation between axle-box acceleration and impact wheel load, especially as regards the high-frequency components. There is thus a strong desire for a more rliable quantification of impact wheel loading in terms of unsprung effective mass, degree and mode of defects, and the mechanical characteristics of vehicle/track dynamics model. This requires actual running tests and more thorough measurements, as well as numerical analysis based on computer models. However, from an engineering viewpoint, a rational design method for PC sleepers involving impact wheel loading is more important, so this should be established first because impact wheel loading (solely composed of a load spike) is entirely different in characteristics from the quasi-static wheel loading (static wheel

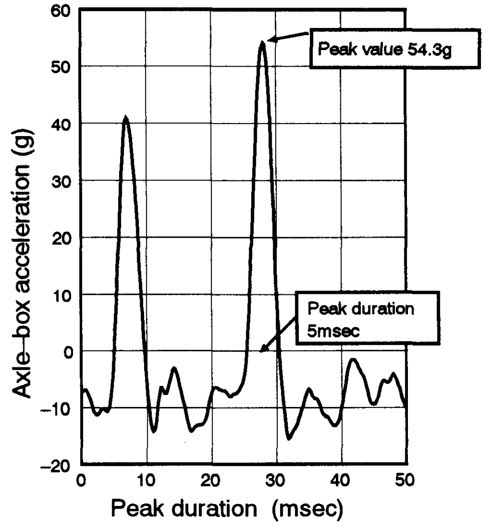

Fig.5 Enlarged-time-scale waveform of axle-box acceleration (railhead corrugation)

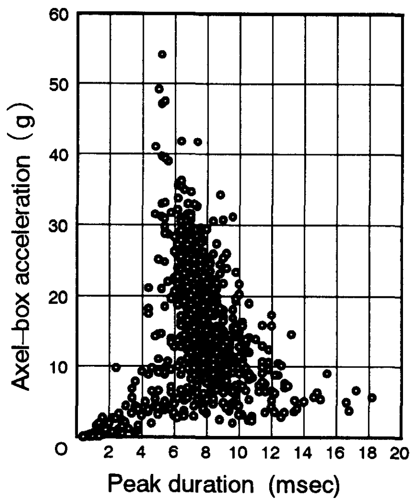

Fig.6 Relationship between shock pulse peak and peak duration (railhead corrugation)

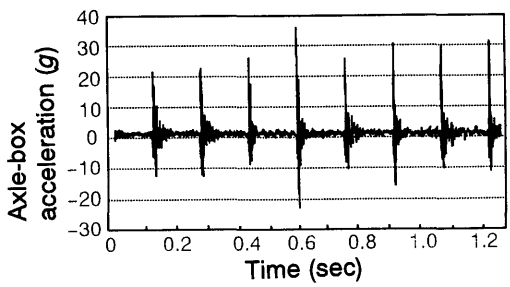

Fig.7 Example of axle-box acceleration waveform (wheel flat)

load + variations) considered by the conventional design technique. The peak values and range of duration are, as we have seen, known to some extent, though such information is not yet well systematized. By resorting to a new design method involving impact wheel load + dynamic response + limit-state behavior instead of the conventional method based on quasi-static wheel load + static response + allowable stress, it will be possible to achieve more cost effective designs for mild loading environments, while, for more severe loading environments, the possibility of mechanical damage can be limited in a rational way.

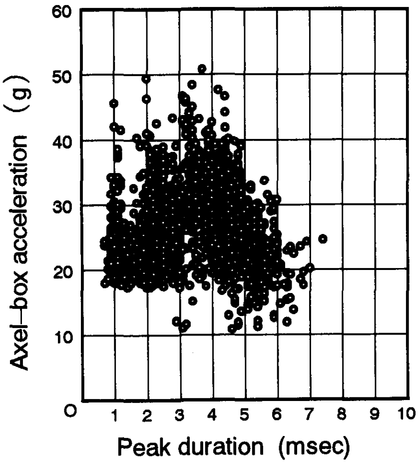

Fig.8 Relatioship between shock pulse peak and peak duration (wheel flat)

4. SURVEY OF IMPACT EFFECT ON PC SLEEPER AND RAIL

To investigate the actual impact effects of wheel flats on a PC sleeper and rail, measurements were conducted of sleeper flexural moment (evaluated from the flexural strain of the bottom surface at the rail seat) and rail flexural moment (evaluated from the flexural strain of the lower flange at the mid-point between the object sleeper and an adjacent sleeper). These measurements were carried out on the Yamanote line with a ballasted track composed of 60kg rail and 3PO type sleepers. By the way, the loading environment on Shinkansen lines is much better than on conventional lines such as the Yamanote line, in spite of the high-speed operation, since wheel flats are by far rarer there.

(1) Measurement Results for Test Train

Figure 9 shows measurements in a case where the maximum flexural moment was recorded both for the PC sleeper and rail, as selected from measured data for the test train referred to in 3. (2). In this case, the wheel flat impacted against the measuring point almost directly. These results were obtained with a running velocity of 28 km/hr, which gave the maximum impact in the test range. The graphs in Fig. 9 offer the following understanding:

1) The quasi-static component of sleeper flexural moment was about 3.5 kNm at maximum when there was no wheel flat, whereas under the direct impact of a wheel flat, it instantaneously reached 17 kNm. The wheel load impact factor (1+i), which represents the ratio between these two values, was 4.9 in this case. The enlarged time-scale waveform indicates that the shock pulse duration was about 5 msec.

2) Just before the wheel flat struck the rail, the wheel tread left the railhead, so the quasi-static component was removed almost completely. Thus it can be supposed that a shock pulse alone acts on the PC sleeper.

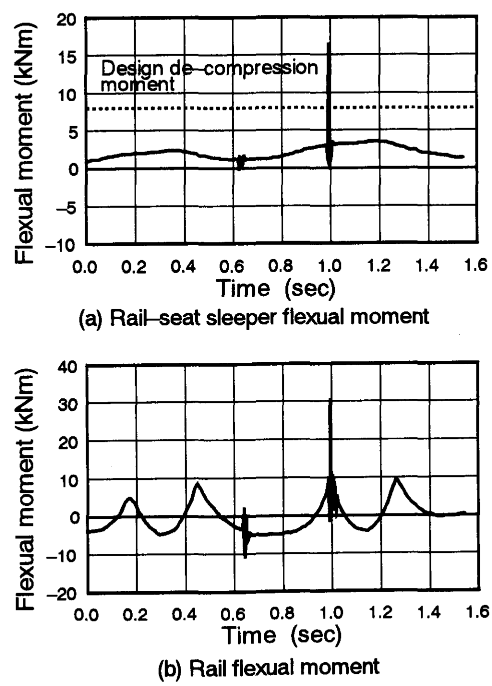

Fig.9 Dynamic response waveform of 3PO type sleeper track produced by wheel flat

3) The quasi-static component of rail flexural moment was about 10 kNm at maximum when there was no wheelflat, whereas under the direct impact of wheel flat, it instantaneously reached 30 kNm. The wheel load impact factor (1+i), which is the ratio between

these two values, was 3.0 in this case. This is significantly smaller than that of the PC sleeper. The enlarged time-scale waveform shows that the duration of this impact pulse was about 10 msec.

(2) Measurement Results for Commuter Train

As of 1986, the 103 series vehicles were still the main stock in use on the Yamanote line, and the use of the 205 series, today's standard, had just started. Wheel flats occurred frequently on the 103 series cars. Though this line is exclusively for commuter trains of relatively light-weight, the loading environment was judged more severe than on other lines due to the wheel flats. So, a survey was implemented on the actual state of rail-seat sleeper flexural moment and rail flexural moment generated by commuter trains (sets of ten electric cars). The measuring location was the same as that of (1) above.

The rail-seat sleeper flexural moment and rail flexural moment peaked for each of the wheel sets. The peak values for 33 commuter trains (total number of wheel sets = 1,320) were determined, to obtain probability curves of flexural moment as shown in Fig. 10. The graphs in this figure indicate that natural wheel flats exert impacts of the same level as the greatest flat artificially produced on the test train. In addition, the graphs illustrate the frequency of high-impact loading.

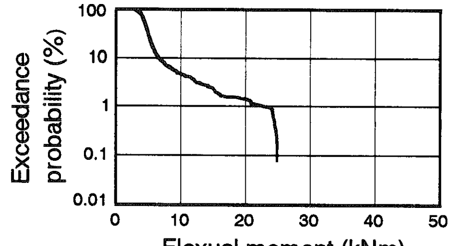

(a) Rail–seat sleeper flexual moment

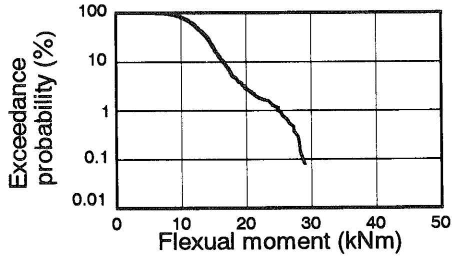

(b) Rail flexual moment

Fig.10 Exceedance probability curve of flexual moments in sleeper and rail

5. DROP-WEIGHT IMPACT TESTS AND FINITE-ELEMENT ANALYSIS FOR DETERMINING DYNAMIC LOADING CHARACTERISTICS OF BALLASTED TRACK WITH PC SLEEPERS

It is technically difficult, at present, to measure in real time the relationship between impact wheel load due to wheel flats and the resulting flexural moments applied to PC sleepers in running tests. Accordingly, simulations were carried out using a drop-weight impact machine with a full-scale test track built in the laboratory, and to provide support in interpreting the simulation tests, finite-element analysis was implemented to quantitatively evaluate and analyze the dynamic loading on PC sleepers caused by impact wheel loads in the form of shock pulses. In these tests, the PC sleepers did not reach the cracking state.

(1) Outline of Drop-weight Impact Tests on Track

The test track spanned a total length of about 10 m. To the railhead on one side, at the mid-point, a shock pulse simulating an impact wheel load was applied by the drop-weight impact machine. The dynamic response of the sleeper just beneath the impact point was measured (Photo 5). As the test track was installed on a concrete bed, a rubber layer (25 mm thick) as commonly used on viaducts with concrete floors was laid as a damper layer. On this rubber layer, a ballasted track of standard structure (ballast under sleeper 250 mm thick) was constructed. There were two different support conditions for the PC sleepers on the ballast: the uniformly supported condition and the center-portion-free state. The latter has been recommended in track maintenance to reduce negative center flexural moment of PC sleepers.

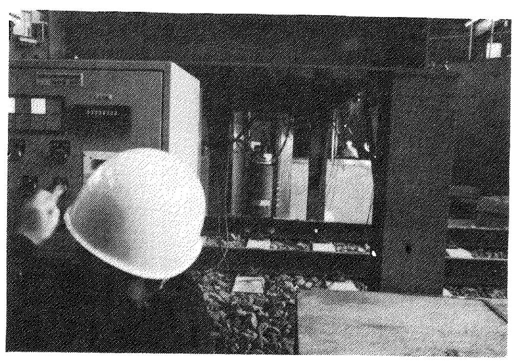

Photo 5 Drop-weight impact test

The peak value of the shock pulse was evaluated as the drop weight mass × the maximum rebound acceleration. It was found possible to set the duration at any value in the range from 1 to 6 msec, as necessary to simulate impact wheel loads induced by wheel flats, by varying the rubber pad thickness (0, 6, 10, 12, 14, 20 mm) placed at the impact point on the railhead and the drop weight mass (62, 110, 160 kg).

(2) Outline of Finite-Element Analysis

The finite-element analysis used plain elements for sleepers; beam elements for rails; bi-linear spring elements, different in stiffness between compressive zone and tensile zone, for rail pads and rail fastenings; and spring-damper elements (linear spring + linear dash pot in parallel) for sleeper base support. Table 1 shows the standard and parametric values of stiffness and damping coefficient used in the analysis for 3PO type sleepers in the uniformly supported condition. The parameter range was determined on the basis of previous test results, etc. The reasons for selecting the listed standard values will be discussed later.

Table 1 Stiffness and damping coefficient used in analysis (3PO type sleeper track ; uniformly supported condition)

Stiffness and damping coefficient	Standard value	Parameter
Stiffness K_{pc} of rail pad and rail fastening (compressive zone)	500 MN/m	100 - 1000 MN/m
Stiffness K_{pt} of rail pad and rail fastening (tensile zone)	75 MN/m	25 - 100 MN/m
Stiffness K_{bs} of sleeper base support (per rail fastening unit)	100 MN/m	50 - 200 MN/m
Damping coefficient C_{bs} of sleeper base support (per rail fastening unit)	50 kNs/m	0 - 200 kNs/m

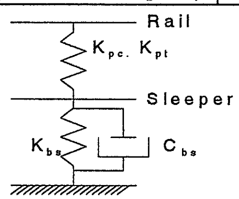

K_{pc}: stiffness of rail pad and rail fastening (compressive zone)

K_{pt}: stiffness of rail pad and rail fastening (tensile zone)

K_{bs}: stiffness of sleeper base support

C_{bs}: damping coefficient of sleeper base support

(3) Comparison between Drop-weight Impact Tests and Finite-element Analysis

Typical examples of measured waveforms obtained in the drop-weight impact tests on track with 3PO type sleepers (uniformly supported condition) are given in Fig. 11 in comparison with the analytical waveforms. The time-step integration technique was utilized in the analysis, with the parameters set to the standard values given in Table 1. These graphs demonstrate the following:

1) The experimental rail-seat load peak value reached about 80% of the impact wheel load peak value. The pulse duration is also about the same (Fig. 11 (b)). For this principal shock pulse, the analysis agreed well with experiment. However, the analysis was unable to match the subsequent response well.

2) Regarding the positive flexural moment in the rail-seat section due to the principal shock pulse, the analysis agreed well with experiment (Fig. 11 (c)). The negative flexural moment in the rail-seat section arising from the subsequent response differs a little between analysis and experiment with respect to peak value and time lag.

3) The negative flexural moment in the mid-span due to the principal shock pulse indicates good agreement between analysis and experiment (Fig. 11 (d)). However, the subsequent response after the principal shock pulse in the analysis has a greater damping effect.

As discussed above, there was good agreement between analysis and experiment for the principal shock pulse which determines the design loads on sleepers. Further, the influence exerted by the analytical parameters was small, as discussed in the next section. From these two findings, we can judge that finite-element analysis is effective as a support method for evaluating the dynamic loading on sleepers due to wheel impact loading.

(4) Effects of Analytical Parameters on Response Waveforms

The case illustrated in Fig. 11 was studied for the influence of analytical parameters on response waveforms in different evaluation items of the track. The analytical results were compared with the experimental data to determine the standard values of analytical parameters. Figure 12 shows the analytical results for flexural moment at the rail seat. These studies revealed the following:

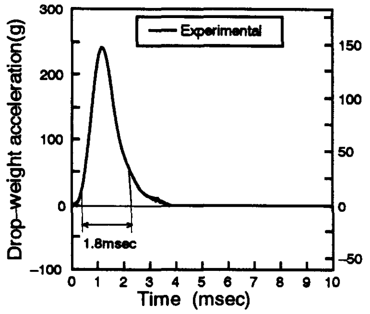

(a) Drop-weight acceleration and impact wheel load

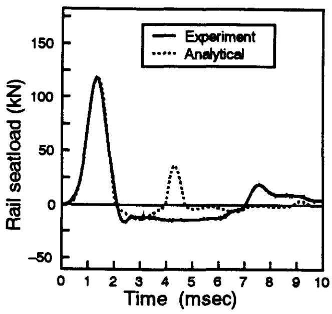

(b) Rail seat load

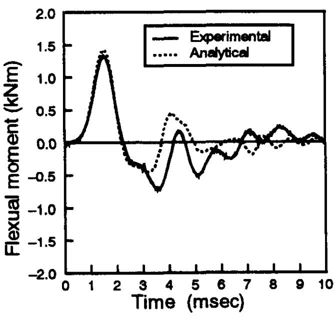

(c) Sleeper flexural moment (rail-seat section)

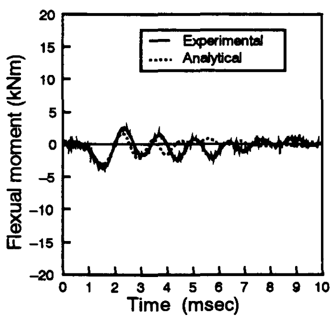

(d) Sleeper flexural moment (mid-span section)

Fig.11 Dynamic response waveform of 3PO type sleeper track

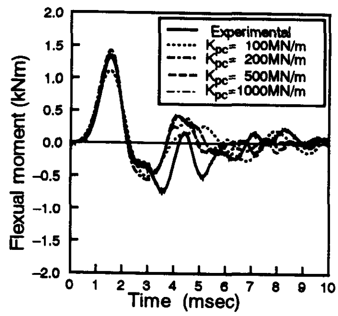

(a) Effect of stiffness K_{pc}

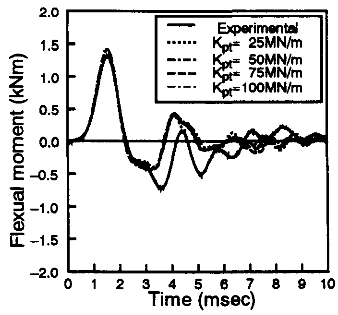

(b) Effect of stiffness K_{pt}

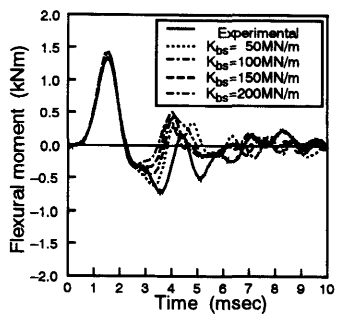

(c) Effect of stiffness K_{bs}

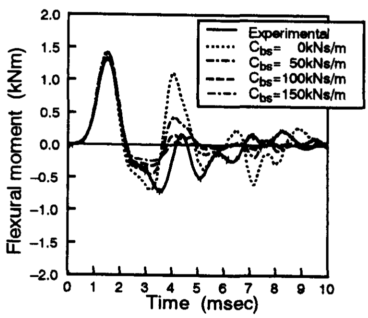

(d) Effect of damping coefficient C_{bs}

Fig.12 Effects of analytical parameter on sleeper flexual moment (rail-seat section of 3PO type sleeper)

1) With the stiffness K_{pc} of the rail pad and rail fastening (compressive zone) set at 100 MN/m, the rail-seat flexural moment was underestimated, whereas at 200 MN/m or more, the influence of the parameter became smaller (Fig. 12 (a)). The stiffness was estimated to be 300 MN/m or more in previous test results. At such high values, the parametric value did not significantly influence the rail-seat flexural moment. In our study, about 500 MN/m was judged appropriate from the rail acceleration (though the corresponding figure is omitted here). Consequently, the standard value of Kpc was taken as 500 MN/m.

2) The stiffness K_{pt} of the rail pad and rail fastening (tensile zone) had very little influence on the rail-seat flexural moment (Fig. 12 (b)).

3) The stiffness K_{bs} of the sleeper base support hardly influenced the principal shock pulse, and its main affect was on the subsequent response of the rail-seat flexural moment (Fig. 12 (c)). Judged from the subsequent response, a stiffness of about 50MN/m was appropriate. But, considering also the results of other evaluation items, the standard value of K_{bs} was set to 100MN/m.

4) The damping coefficient C_{bs} of the sleeper base support had little effect on the principal shock pulse, but it influenced the subsequent response (Fig. 12 (d)). From the magnitude of remaining vibration component, the standard value of C_{bs} was taken as 50 kNs/m.

(5) Effects of Impact Wheel Load Duration on Sleeper Flexural Moment, etc. (Single-sided Loading)

Figure 13 shows a comparison between experimental and analytical results, when impact wheel loads with different duration were applied to track with 3PO type sleepers (uniformly supported condition). The static burden values (analytical) given in Fig. 13 were obtained using, as the static values of analytical parameters, 100 MN/m for K_{pc} (compressive zone) and 50 MN/m for K_{bs}. The graphs in Fig. 13 demonstrate the following:

1) The static ratio of rail-seat load / wheel load was about 40%, whereas its maximum, at a duration of about 1.5 msec, was about 85% (experimental) against about 75% (analytical) (Fig. 13 (a)).

2) The positive rail-seat flexural moment took on a dynamic maximum value at a duration of about 1.5 msec, and it reached about twice that under static loading in the analysis (Fig. 13 (b)). This magnitude under dynamic loading of twice the static loading moment can be explained as follows. The moment is magnified by about 1.4 as a result of the change in K_{pc} from 100 MN/m (static) to 500 MN/m (dynamic), and magnified again by a factor of about 1.4 due to a resonance from impact wheel load. Since the eigen frequency of the vibration mode (Fig.14) governing the positive rail-seat flexural moment is 500 to 700 Hz (eigen period: 2 to 1.5 msec), it can be estimated that, when the impulse duration approaches this eigen period range, that is, around 1.5 msec, a resonance with a magnification factor of about 1.4 occurs (Fig.15). It is a known phenomenon that the moment applied to PC sleepers due to wheel flats, after reaching a maximum at a low speed of around 30 km/h, again rises at higher speeds above about 200 km/h [3,5]. This phenomenon is attributable to dynamic loading effects, coupled with the 1

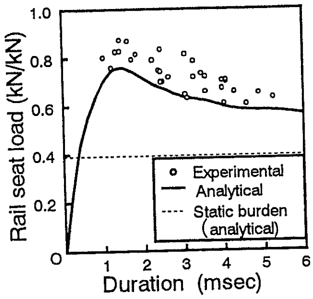

(a) Rail-seat load

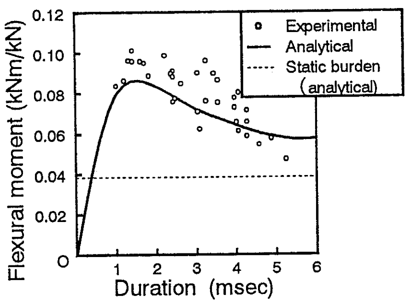

(b) Positive rail-seat flexural moment

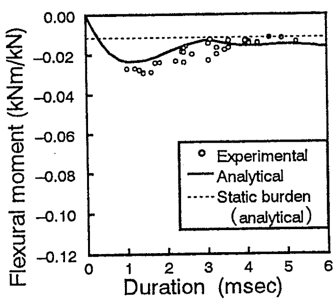

(c) Negative center flexural moment

Fig.13 Effect of duration of unit impact wheel load on sleeper flexural moments,etc. (single-sided loading) to 2 msec of high impact wheel load induced by wheel flats in the high-speed range.

3) The negative center flexural moment reached a dynamic maximum when the duration was 1 msec. This was analytically about twice the static moment value (Fig. 13 (c)).

(6)Effects of Ballast Support Conditions on Sleeper Flexural Moment

Similar studies to those for the uniformly supported condition as discussed in (5) were implemented for the "center-portion-free condition", and the following understanding was obtained (the corresponding figures are omitted here):

1) The change to center-portion-free condition had almost no influence upon the dynamic characteristics of the positive rail-seat flexural moment.

2) The negative center flexural moment tended to converge to a small static value for the center-portion-free condition as the impulse duration became longer than some 3 msec, but at around 1 msec, the dynamic maximum moment was almost the same as that under the uniformly supported condition shown in Fig. 13 (c). Thus, the center-portion-free condition was seen to have almost no effect on reducing the negative center flexural moment under impulsive loading.

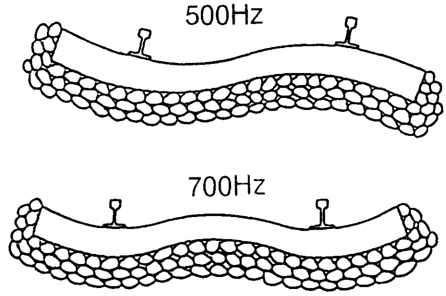

Fig.14 Eigen-modes governing sleeper flexual moment (rail-seat section)

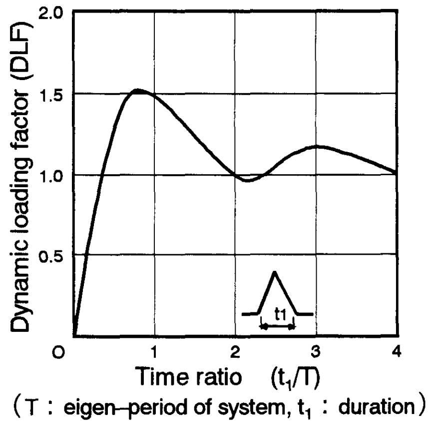

Fig.15 Effect of duration on response of one-degree-of-freedom system (T:eigen-period of system; t_1:duration)

(7) Effect of Impact Wheel Load Duration on Sleeper Flexural Moment (simultaneous symmetric loading)

Wheel flats usually form at almost the same point on wheels on both sides. Thus the impact load may be applied symmetrically. Since the drop-weight impact machine is capable of single-sided loading only, the effects of simultaneous symmetric loading were investigated through analysis of a case where wheel shock pulses were applied symmetrically to both rails at the same time. Figure 16 illustrates the relationships between sleeper flexural moment per impact wheel load of 1kN and duration on track with 3PO type sleepers (uniformly supported condition). The graphs in Fig. 16 demonstrate the following:

1)The positive rail-seat flexural moment under simultaneous symmetric loading was of the same level as single-sided loading (Fig. 16 (a)).

2)The negative center flexural moment under simultaneous symmetric loading was naturally twice that of single-sided loading for different duration (Fig. 16 (b)).

3) The negative rail-seat flexural moment induced by the rebound response under simultaneous symmetric loading reached a maximum when the duration was about 1 msec. The maximum value was about 80% of the maximum positive rail-seat flexural moment under single-sided loading, as shown in Fig. 16 (c).

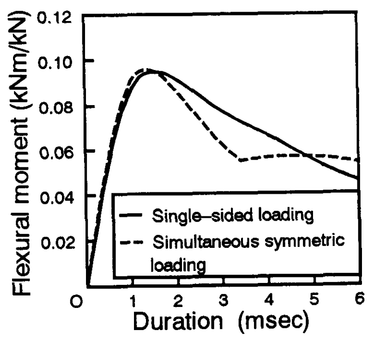

(a) Positive rail-seat flexual moment

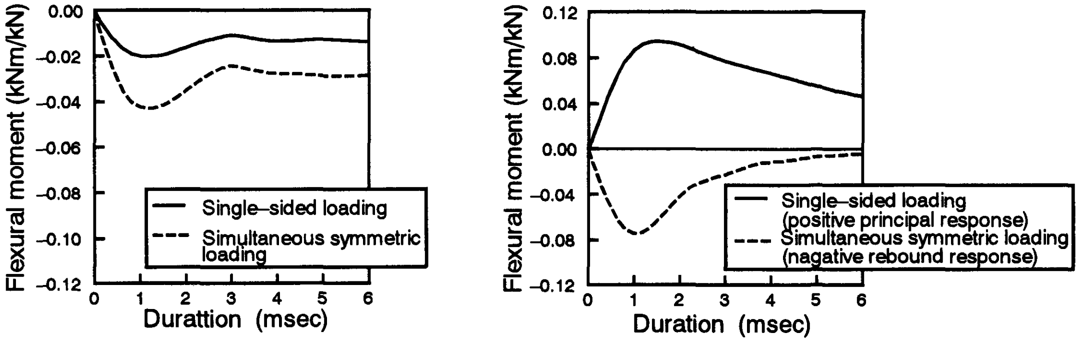

(b) Negative center flexual moment

(c) Negative rail-seat flexual moment

Fig.16 Effect of duration of unit impact wheel load on sleeper flexual moments (simultaneous symmetric loading)

6. DISCUSSION ON DESIGN SLEEPER FLEXURAL MOMENT FROM VIEWPOINT OF LIMIT-STATE DESIGN METHOD

(1) Experiment on Relationship between Sleeper Flexural Moment and Impact Wheel Load

In the drop-weight impact tests using full-scale test tracks assembled in the laboratory, the fall height was increased step by step up to the maximum available height in investigating the relationship between sleeper flexural moment and impact wheel load. The results discussed below concern track with 3PO type sleepers, representative of narrow gauge track, and track with 4T type sleepers, representative of standard gauge. By suitably combining a 160 kg weight and rubber pads (varying the total pad thickness) on the railhead at the impact point, the duration of wheel load impact was kept almost constant at about 4 mesc, regardless of the fall height and test track type.

a) Positive Rail-seat Flexural Moment

The experimental line and the new design line expressing the relationship between positive rail-seat flexural moment and wheel impact load, are drawn in Fig. 17 for both tracks. This figure also shows the conventional design line and the de-compression moment based on the conventional design technique using quasi-static wheel load (see 2. (1) and Fig. 1). The experimental line represents the positive rail-seat flexural moment obtained from the flexural strain at the top surface, involving the section properties with whole sectional area assumed effective. The flexural moment resulting from the experimental line is overestimated after a crack starts in the bottom surface. Hence, assuming that the rail-seat flexural moment increases in linear proportion to the impact wheel load, the new design line was set as an extrapolated estimation line. Figure 17 demonstrates the following:

1) The flexural moment per unit wheel impact load by the new design line agrees, in general, with the analytical value (shown in Fig. 13 (b) only for the 3PO type sleeper) of dynamic loading characteristics for a duration of 4 msec.

2) There is no significant difference between the new design line for narrow gauge track and that for standard gauge. For both gauges, the rail-seat flexural moments were estimated at about 28kNm under an impact wheel load of 400 kN.

3) Though a large value, 0.6, was used for the conventional design lines as the wheel load distribution factor df, the flexural moments were underestimated compared with those by the new design lines for the same wheel load.

4) When the maximum impact wheel load is taken as 400 kN, a flexural moment 3.0 times the de-compression moment given by the conventional design may be applied in the ultimate limit-state to the 3PO type sleeper, and a flexural moment 2.8 times to the 4T type sleeper.

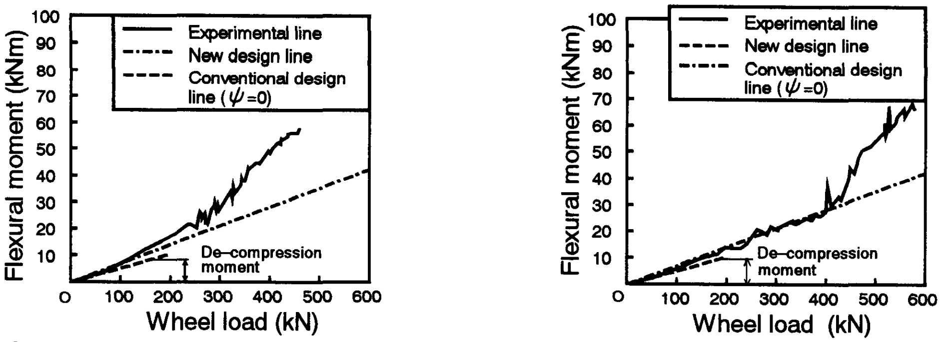

(a) 3PO type sleeper track for narrow gauge
(b) 4T type sleeper track for standard gauge

Fig.17 Relationship between positive rail-seat flexual moment and wheel load

b) Negative Center Flexural Moment

Figure 18 shows the experimental line, the new design line, and the new design line × 2 for both tracks, expressing the relationship between negative center flexural moment and impact wheel load. Figure 18 also includes the conventional design line and the de-compression moment drawn by the method discussed in 2. (1) (see Fig. 1) involving the quasi-static wheel load. The experimental line represents the negative center flexural moment obtained from the flexural strain at the top surface, using the section properties with whole sectional area assumed effective. The flexural moment resulting from the experimental line is overestimated after a crack starts in the mid-span top surface. Hence, assuming the flexural moment increases in linear proportion to the impact wheel load, the new design line was set as an extrapolated estimation line. The new design line × 2 represents the flexural moment under simultaneous symmetric loading. Figure 18 demonstrates the following:

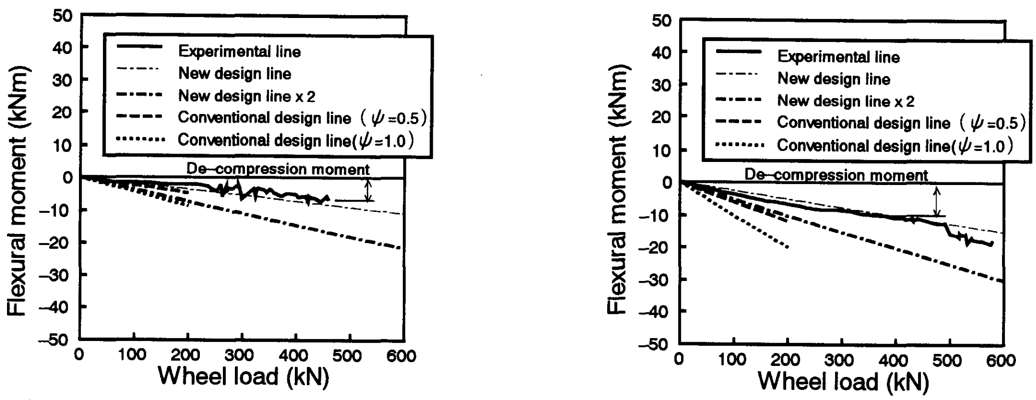

(a) 3PO type sleeper track for narrow gauge
(b) 4T type sleeper track for standard gauge

Fig.18 Relationship between nagative center flexual moment and wheel load

1) The flexural moment per unit wheel impact load by the new design line agrees, in general, with the analytical values (shown in Fig. 13 (c) only for the 3PO type sleeper) of dynamic loading characteristics for a duration of 4 msec.

2) By the new design lines, the flexural moment for standard gauge track is 1.5 times that for narrow

gauge. The flexural moment under an impact wheel load of 400 kN was estimated at about -6.4 kNm for the 3PO type sleeper, and about -9.6 kNm for the 4T type sleeper.

3) The new design line × 2 shows values near those of the conventional design line with ψ =1.0 for narrow gauge, and, near those of the conventional design line with ψ =0.5 for standard gauge.

4) When the maximum impact wheel load is taken as 400kN × 2 (simultaneous symmetric loading), a flexural moment 2.1 times the de-compression moment given by the conventional design may be applied in the ultimate limit-state to both the 3PO type and 4T type sleepers.

(2) Discussion on Design Sleeper Flexural Moment

a) Prediction Formulas for Sleeper Flexural Moment

1) As for the relationship between positive rail-seat flexural moment M and impact wheel load, Equation 2 can be used both for narrow and standard gauges. This equation was obtained by making the new design line in Fig. 17 dimensionless in static wheel load P_{st}, using impact wheel load = $P_{st} \cdot (1+i_d)$.

For narrow and standard gauges:

$$M/P_{st} = 0.07 \cdot (1+i_d) \qquad \text{(Eq.2)}$$

2) As for the relationship between negative center flexural moment M and impact wheel load, Equation 3 can be used for narrow gauge and Equation 4 for standard gauge. These equations were obtained by making the new design line × 2 in Fig. 18 dimensionless in static wheel load P_{st} .

For narrow gauge: $M/P_{st} = 0.032 \cdot (1+i_d)$ (Eq. 3)

For standard gauge: $M/P_{st} = 0.048 \cdot (1+i_d)$ (Eq. 4)

As mentioned in 2. (1), the conventional design method introduces nominal factors such as the wheel load distribution factor d_f and the center binding coefficient ψ to evaluate the static flexural moment, with a fixed wheel load impact factor $(1+i_d)$ underestimated. In contrast, Equations 2 to 4, which eliminate the nominal factors, are proposed to easily evaluate the dynamic flexural moment, on the assumption that it is more important to determine an appropriate value or appropriate value range of $(1+i_d)$ for each limit-state in different loading environments.

b) Setting Design Sleeper Flexural Moment

A study of the relationships between sleeper flexural moment and impact wheel load leads to the following considerations to determining design sleeper flexural moment:

1) Equations 2 to 4 were obtained for a duration of impact wheel load of about 4 msec. When the duration is shorter than 4 msec, as explained in 5. (5), the sleeper flexural moment is likely to be magnified further by up to 40% because of the resonance effect. It should therefore be noted that the sleeper flexural moment obtained from Equations 2 to 4 may be somewhat underestimated, especially in the ultimate limit-state. However, in practice, it is more essential to suitably determine the maximum value of wheel load impact factor $(1+i_d)$ for the ultimate limit-state. It is at present difficult to definitely determine this maximum value. It might be said, for reference purposes, that a suitable value is approximately 5, judged from the currently available measured and estimated data.

2) For evaluating the sleeper flexural moment in the serviceability limit-state and fatigue limit-state, Equations 2 to 4, which are reasonable in terms of duration, can be applied as they are. It should be understood, however, that the cumulative frequency distribution curve of wheel load impact factor $(1+i_d)$ spans the range from a minimum value corresponding to the actual static load to almost the maximum value for the ultimate limit-state.

7. LOAD CARRYING CAPACITY OF PC SLEEPERS IN SERVICEABILITY LIMITE-STATE

(1) Outline of Repetitive Impact Loading Test on Single Sleepers

To investigate the cracking of a PC sleeper which has experienced repeated impact wheel loading, a single sleeper was mounted on the drop weight impact machine, as shown in Photo 6, to conduct a repetitive impact loading test on the rail-seat section under constant impulsive loading for each specimen. The number of repetitions was set at 17,000 at maximum. Though this was an upper limit imposed by the available test period, it was in fact adequate for comparing pre-tensioned sleeper and post-tensioned sleepers. The drop weight mass used was 62 kg. At the impact point on the rail seat, an iron plate (20 mm thick) and a rubber pad (16 mm thick) were placed as a damper. This test set-up was capable of applying impulsive flexural moment lasting about 4 msec to the sleeper, which generated a suitable loading rate in strain equivalent to an actual situation where wheel flats strike the track. As for the sleeper loading conditions, the flexural strain at the top surface at the rail-seat section was measured. Based on this flexural strain, sleeper flexural moment and impact wheel loading were estimated using the relationship shown in Fig.17 obtained from the drop-weight impact test on the track. The test results are discussed below for two pre-tensioned 3PR type sleepers and four post-tensioned 3PO type sleepers. The latter sleepers were made by unbonded post-tensioning.

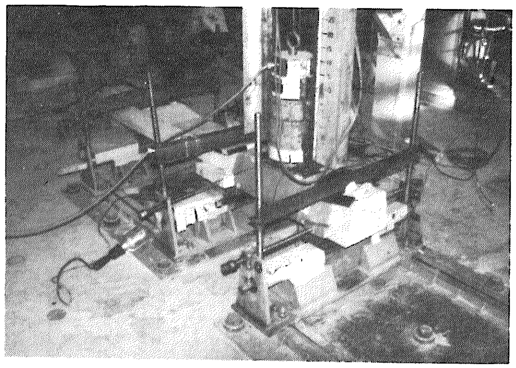

Photo 6 Single-sleeper repetitive impact loading test

(2) Loading Conditions and Cracking States of Test Specimens

Table 2 summarizes the loading conditions of the test specimens and results of a cracking assessment. Figure 19 shows the evolution of remaining crack width (measured with a contact gauge) for the maximum flexural crack in the rail-seat section. Examples of cracking after the tests are shown in Photo 7. These results reveal the following for each type of test specimen:

Table 2 Specimen loading conditions and evaluation of cracking states

Impact wheel load (kN)	210	240	270	330	De-compression moment (kNm)
Flexural moment applied (kNm)	14.7	16.8	18.9	23.1	
No. of repetitions	17,000	17,000	17,000	17,000	
Pre-tensioned 3PR type			C-1 ◎	C-2 △	8.0
Post-tensioned 3PO type	C-3 O	C-4 △	C-5 ×	C-6 ××	9.4

◎: Cracking state well within allowable range for serviceability limit-state
O: Cracking state generally within allowable range
△: Cracking state slightly exceeding allowable range
×: Cracking state definitely exceeding allowable range
××: Cracking state progressing to rupture (No. of repetitions=1,757)

1) In the case of C-1 (pre-tensioned 3PR type, 270 kN impact wheel load), only very tiny flexural cracks were produced in the bottom surface at the rail-seat section. The remaining crack width was almost zero after 17,000 impact repetitions. The cracking state was judged as well within the range allowable for the serviceability limit-state.

2) In the case of C-2 (pre-tensioned 3PR type, 330 kN impact wheel load), crack development was more notable than with C-1. The remaining crack width reached about 0.07 mm after 17,000 impact repetitions. However, no slipping of strand was observed, which re-confirmed the excellent bonding performance of the indented prestressing strands. As a global evaluation, the cracking state was assessed to be slightly over the range allowable for the serviceability limit-state.

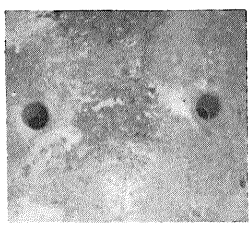

(a) C-1 (pre-tensioned 3PR type; 270 kN impact wheel load)

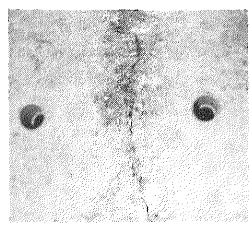

(b) C-5 (post-tensioned 3PO type; 270 kN impact wheel load)

Photo 7 Cracking states after test

3) In the case of C-3 (post-tensioned 3PO type, 210 kN impact wheel load), fine flexural cracks occurred, but the remaining crack width was almost zero after 17,000 impact repetitions. The cracking state was evaluated to be, in general, within the range allowable for the serviceability limit-state.

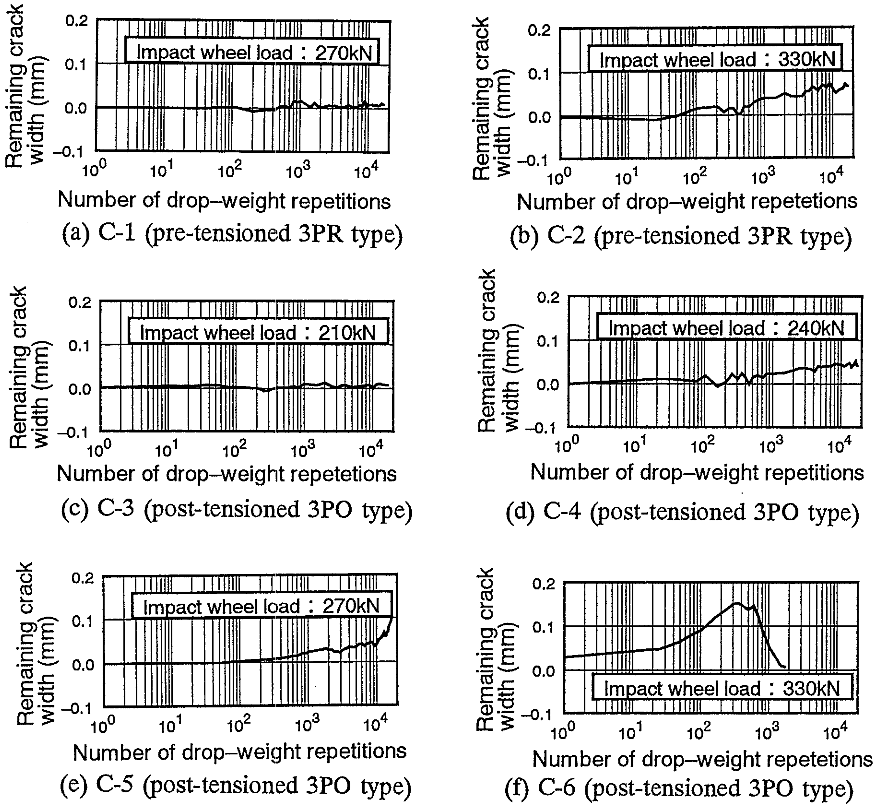

(a) C-1 (pre-tensioned 3PR type)

(b) C-2 (pre-tensioned 3PR type)

(c) C-3 (post-tensioned 3PO type)

(d) C-4 (post-tensioned 3PO type)

(e) C-5 (post-tensioned 3PO type)

(f) C-6 (post-tensioned 3PO type)

Fig.19 Evolution of remaining crack width

4) In the case of C-4 (post-tensioned 3PO type, 240 kN impact wheel load), flexural cracking was more notable than with C-3, with the remaining crack width reaching about 0.05 mm after 17,000 impact repetitions. In general, as with C-2, the cracking state was assessed to slightly exceed the range allowable for the serviceability limit-state.

5) In the case of C-5 (post-tensioned 3PO type, 270 kN impact wheel load), damage in the form of a groove was produced (Photo 7 (b)). The remaining crack width reached about 0.1 mm after 17,000 impact repetitions, and the tendency was toward further increase. In general, the cracking state was judged to significantly exceed the range allowable for the serviceability limit-state.

6) In the case of C-6 (post-tensioned 3PO type, 330 kN impact wheel load), bottom and side concrete along the dominant flexural crack peeled off, and the damage propagated to the upper section. Consequently, the test was stopped at 1,757 impact repetitions, with the conclusion that rupture was developing.

(3) Comparison of Pre-tensioned and Post-tensioned Types

From the loading conditions of test specimens and the cracking state evaluations summarized in Table 2, the following points relating to the serviceability limit-state design of the pre-tensioned and post-tensioned (unbonded) sleepers were verified.

1) As for the pre-tensioned 3PR type, the C-1 specimen exhibited cracking which was well within the range allowable for the serviceability limit-state under a burden 2.3 times the de-compression moment.

2) As for the post-tensioned 3PO type, the C-3 specimen exhibited cracking which was assessed to be just outside the range allowable for the serviceability limit-state under a burden 1.6 times the de-compression

moment.

3) When comparing the impact wheel loads between 3PR and 3PO types, and referring to the specimens exhibiting the almost equal cracking states, we obtained the ratios :

(C-1)/(C-3) = 1.30, (C-2)/(C-4) = 1.37

4) From 1) to 3) above, it can be inferred that, from the viewpoint of restricting damage to similar cracking states at the serviceability limit-state, the de-compression moment of post-tensioned type (unbonded) should be at least 30% larger than that of pre-tensioned type.

8. LOAD CARRYING CAPACITY OF PC SLEEPERS IN FATIGUE LIMIT-STATE

(1) Types of PC Sleepers evaluated for Fatigue Lifetime

By studying the rail-seat section behavior of typical PC sleepers used for JR lines (Fig. 2), the fatigue lifetime as determined by prestressing steel rupture was evaluated. Post-tensioned sleepers manufactured in Japan are usually of unbonded type. However, this study of bonded types assumes that the prestressing rods are completely bonded to the concrete. Since in general the fatigue life of bonded tendons is shorter, this assumption tends to offer conservative evaluation.

(2) Prediction Method of Fatigue Lifetime

a) Calculation of Prestressing Steel Stress under Impact Wheel Loading

The relationship between prestressing steel stress and sleeper flexural moment was investigated by computing stresses in the cross section of PRC (prestressed reinforced concrete) on the following assumptions:

1) Sectional strain is linearly distributed.

2) Prestressing steel is completely bonded to concrete.

3) Tensile strength of concrete is zero.

The calculation was found to be approximately effective for impulsive loading, based on the results of a single-sleeper impact loading test with a pre-tensioned 7PR type specimen (the corresponding figure is omitted here). Impact wheel load was estimated from sleeper flexural moment using Equation 2.

b) Fatigue Strength of Prestressing Steel against Stress Amplitude

Study on fatigue strength of prestressing steel against stress amplitude should consider loading rate in strain. However, because such data are not available at present, static fatigue strength was used in this preliminary step of the investigation, as follows:

1) The fatigue strength of indented prestressing strands consisting of three wires 2.9 mm in each diameter as used in pre-tensioned PC sleepers was reported by Iwasaki and Asanuma [11] and these are marked with circles in Fig. 20. In this case, the sustained stress of test specimens was set at the effective prestressing level of the pre-tensioned types. As shown in Fig. 20, an S-N diagram was constructed, using a straight line to approximate the three data plots in the logarithmic

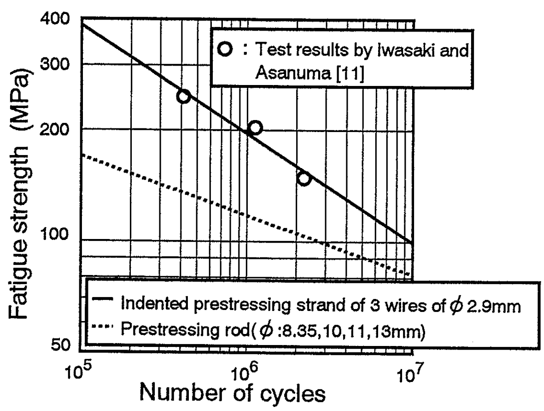

Fig.20 Fatigue strength of prestressing steel

coordinates.

2) For the fatigue strength of prestressing rods, an S-N diagram was constructed, as shown in Fig. 20, on the basis of the design equation given in Japanese .Design Standards for Railway Structures (Concrete Structures). When applying the design equation, the value of sustained stress / tensile strength was set to 0.56, which corresponds to the effective prestressing level of the post-tensioned type.

(3) Prediction Results of Fatigue Lifetime

The fatigue lifetime prediction results in terms of prestressing steel rupture are illustrated in Fig. 21. The results reveal the following:

1) Both for pre-tensioned and post-tensioned (bonded) sleepers, the fatigue lifetime varies considerably with prestressing steel amount and effective prestressing level. Considering also that the fatigue lifetime required for PC sleepers may be several hundred million cycles, the fatigue of prestressing steel induced by impact wheel loads may govern their design.

2) By comparing the behavior of fatigue lifetime prediction curves, it was determined that the lifetime of post-tensioned types (bonded) tends to decrease more abruptly than that of pre-tensioned types as impact wheel load increases. This is because the low-cycle fatigue strength of the prestressing rods is set much lower than that of the prestressing strands.

(4) Verification of Lifetime Prediction Results by Fatigue Testing of PC Sleepers

For comparison purposes, static fatigue test data of the earlier studies on pre-tensioned 3T type sleepers are plotted in Fig. 22 along with the fatigue lifetime prediction curve in Fig. 21 (a). The static fatigue test data, which relate to sleepers on the Tokaido Shinkansen line, comprise test results on specimens sampled 7 years after the start of service, as well as those of specimens sampled 20 years after the start of service and unused specimens exposed for 20 years [12]. The static fatigue data were obtained by converting sleeper flexural moment to impact wheel load using Equation 2. Therefore, since the same flexural-moment-to-impact-wheel-load relationship is involved for both the experimental data and the prediction results, it is possible to directly compare the experimental data with the fatigue lifetime prediction curve in terms of impact wheel load. It should be noted, however, that the influence of loading rate in strain on the fatigue strength of prestressing steel was ignored both in the experimental and predicted data. Figure 22 offers the following understanding:

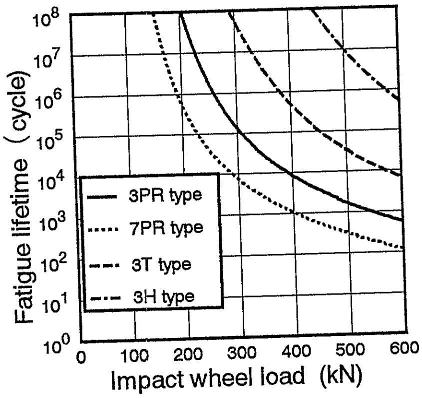

(a) Pre-tensioned type

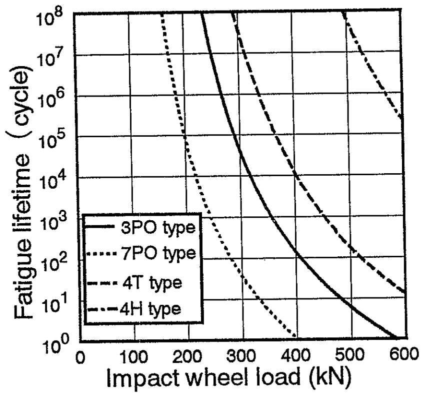

(b) Post-tensioned(bonded) type

Fig.21 Fatigue lifetime of PC sleepers (Positive rail-seat flexual moment)

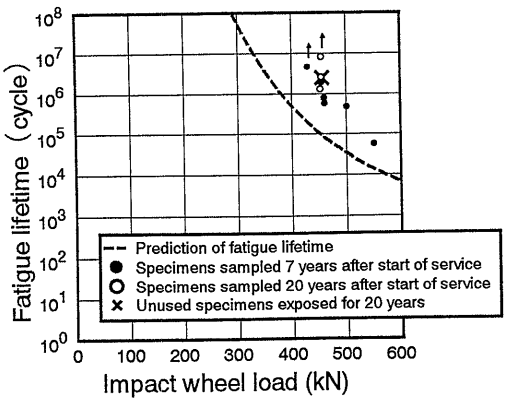

Fig.22 Fatigue lifetime of pre-tensioned 3T type sleeper (positive rail-seat flexual moment)

1) The fatigue lifetime prediction curve tended to become more conservative than the experimental data in higher cycle range. One of the reasons for this is that the actual fatigue strength of the prestressing strands is likely to be higher than the set strength in Fig. 20.

2) Through a series of fatigue tests, it was confirmed that PC sleepers used for 20 years on the Tokaido Shinkansen line have equal remaining fatigue lifetime to unused sleepers.

9. LOAD CARRYING CAPACITY OF PC SLEEPERS IN ULTIMATE LIMIT-STATE

(1) Results of Impact Ultimate Flexural Capacity Tests

In the impact loading tests on track and single sleepers, where the height from which a drop-weight fell was increased step by step up to the maximum available height, no failure occurred in any case. The maximum impulsive loading applied to the pre-tensioned 3PR type sleepers and post-tensioned 3PO type sleepers (unbonded) was estimated to be, when converted to an impact wheel load, 520 kN. When converted to a sleeper flexural moment, it was estimated to be 36.4 kNm. However, the static flexural capacity is no more than 28.4 kNm (3PR type) and 26.4 kNm (3PO type). Therefore, the specimens did not fail under the sleeper flexural moment, which is 40% or more larger than the static flexural capacity.

(2) Types of PC Sleepers evaluated for Ultimate Flexural Capacities

From the test results, it was inferred that an increase in material strength due to high loading rate in strain contributes to ultimate flexural capacity under impulsive loading. Accordingly, the authors reviewed the evaluation method used for impulsive ultimate flexural capacity, looking for a more suitable design practice in the ultimate limit state. In this review, the behavior of the rail-seat section of typical JR sleepers (Fig.2) was studied. For post-tensioned sleepers, the bonded type was considered again, assuming that the prestressing steel is completely bonded to the concrete. Because the static ultimate flexural capacity of the unbonded type is, in some cases, about 30% smaller than that of the bonded type [13], the evaluation result here is likely to be on the risky side for the unbonded type.

(3) Evaluation Method of Impulsive Ultimate Flexural Capacity

a) Dynamic Stress-strain Curves of Concrete

Referring to the recent research results by Takahashi [14], the dynamic stress-strain curves of the concrete were determined as follows:

1) The dynamic stress σ-to-strain ε curve of concrete is expressed by the parabolic equation below, based on the dynamic compressive strength ${}_df'_c$ and dynamic ultimate compressive strain ${}_d\varepsilon_{co}$.

$$\sigma = {}_df'_c\,[2(\varepsilon / {}_d\varepsilon_{co}) - (\varepsilon / {}_d\varepsilon_{co})^2] \qquad \text{(Eq. 5)}$$

2) The dynamic compressive strength ${}_df'_c$ of concrete is given by Equation 6, factoring in the static compressive strength ${}_sf'_c$ and loading rate in strain $\dot{\varepsilon}$.

$${}_df'_c / {}_sf'_c = 1.49 + 0.268\,(\log \dot{\varepsilon}) + 0.035\,(\log \dot{\varepsilon})^2 \qquad \text{(Eq. 6)}$$

3) The dynamic ultimate compressive strain of concrete ${}_d\varepsilon_{co}$ is given by Equation 7, on the basis of the static ultimate compressive strain ${}_s\varepsilon_{co}$ ($=3500\times10^{-6}$) and loading rate in strain $\dot{\varepsilon}$.

$${}_d\varepsilon_{co} / {}_s\varepsilon_{co} = 1.24 + 0.053\,(\log \dot{\varepsilon}) \qquad \text{(Eq. 7)}$$

4) The loading rate in strain of the concrete $\dot{\varepsilon}$ is taken as 2. This is an approximate value obtained by assuming that the duration for which the sleeper flexural moment acts is 4 msec and, accordingly, that the strain ε reaches about $4{,}500\times10^{-6}$ ($={}_d\varepsilon_{co}$) in 2 msec.

5) The dynamic stress-strain curves of concrete based on 1) through 4) above are shown in Fig. 23.

b) Dynamic Stress-strain Curves of Prestressing Steel

The dynamic stress-strain curves of the prestressing steel were constructed as mentioned below, referring to recent research results on reinforcing bars, etc. by Takahashi [14]. The data on which the proposed equation is based include no data on prestressing steel. Thus, the effect of loading rate in strain on the strength of prestressing steel is likely to be overestimated. This point should have been verified, but such a verification could not be carried out within the scope of this research. In consequence, the evaluation of impact ultimate flexural capacity discussed below is no more than qualitative. It should therefore be quantitatively reviewed in a future study.

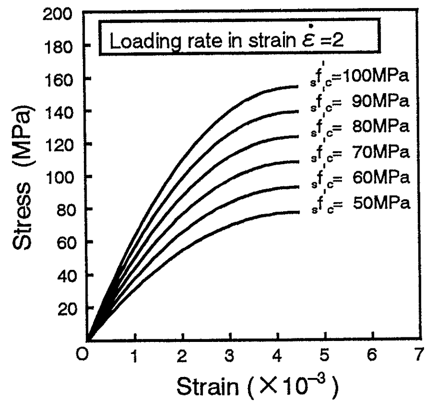

Fig.23 Dynamic stress - strain curve of concrete

1) The elastic modulus up to the upper yield point is assumed to be equal to the static modulus of elasticity, and not influenced by the loading rate in strain.

2) The upper yield point stress $_df_{y,u}$ is given by Equation 8 on the basis of the static upper yield point stress $_sf_{y,u}$ and loading rate in strain $\dot{\varepsilon}$. $_sf_{y,u}$ is assumed to be set at 0.84 times the design tensile strength f_{pud}.

$$_df_{y,u}/\ _sf_{y,u} = 10^{0.380\log\dot{\varepsilon}-0.258} + 0.993 \qquad \text{(Eq. 8)}$$

3) The loading rate in strain $\dot{\varepsilon}$ of prestressing steel is assumed to be set at 6 for the strands and 3 for the rods. These values were determined by assuming that the duration for which the sleeper flexural moment acts is 4 msec and, accordingly, that the stress rises from the effective prestressing level to the upper yield point stress $_df_{y,u}$ in 2 msec, based on assumptions 1) and 2).

4) The dynamic stress-strain curves of prestressing steel based on 1) through 3) above are shown in Fig. 24.

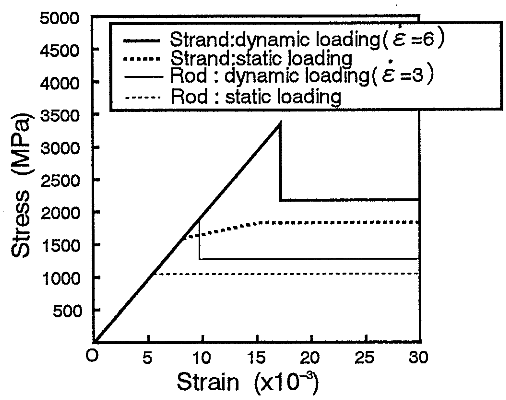

Fig.24 Dynamic stress-strain curve of prestressing steel

c) Other Assumptions in evaluating Impulsive Ultimate Flexural Capacity

In evaluating the impulsive ultimate flexural capacity, the following commonly adopted assumptions were resorted to, in addition to the conditions described in a) and b):

1) Sectional strain is linearly distributed.

2) Effective prestressing stress of prestressing steel alone is considered as the initial stress, and the initial stress in the concrete is ignored.

d) Evaluated Ultimate Flexural Capacities

As shown in Fig. 25 and described below, the static ultimate flexural capacity (S) and impulsive ultimate flexural capacity (I_1, I_2) were evaluated.

1) Static ultimate flexural capacity S: this is a value reached when concrete fails in the compressive zone after the prestressing steel undergoes tensile yield.

2) Impulsive ultimate flexural capacity before upper yield point I_1 : this is a value reached when concrete fails in the compressive zone before the prestressing steel reaches the upper yield point.

3) Impulsive ultimate flexural capacity at upper yield point I_2 : this is a value reached when concrete does not fail in the compressive zone with the prestressing steel attaining the upper yield point.

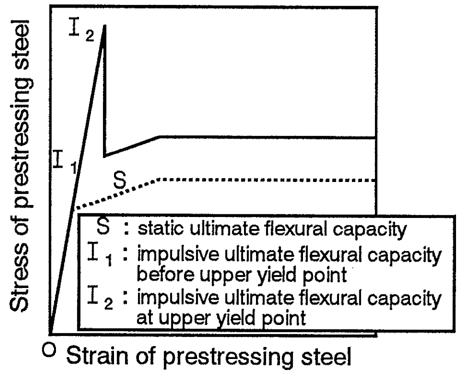

Fig.25 Difinition of impulsive ultimate flexual capacities in terms of rupture modes

At a level lower than the capacity I_2, there exists another impulsive ultimate flexural capacity at the lower yield point. But, as this fracture mode occurs after I_2 is reached, its study was omitted.

(4) Comparison of Impulsive Ultimate Flexural Capacity Modes between Pre-tensioned and Post-tensioned Types

Impulsive ultimate flexural capacity modes were studied at the rail-seat section of the pre-tensioned 3PR type and post-tensioned 3PO type (unbonded). The study results are depicted in Fig. 26. The lines in each graph represent the flexural capacity as a function of prestressing steel stress in the lowest row, for the different $_{s}f'_{c}$ set values (50 to 100 MPa). The uppermost point of each line denotes compressive failure of the concrete. The uppermost point marked ＊ means termination of analysis (in the case where concrete did not undergo compressive failure). Figure 26 also shows, with the actual concrete strength of current sleepers taken as $_{s}f'_{c}$ = 60 MPa, an + mark representing the static ultimate flexural capacity S, and the impulsive ultimate flexural capacities shown I_1 (impulsive ultimate flexural capacity before upper yield point) and I_2 (impulsive ultimate flexural capacity at upper yield point). These results reveal the following:

1) The impulsive ultimate flexural capacity is given by I_1 for the pre-tensioned type, whereas it is given by I_2 for the post-tensioned type.

2) The influence of $_{s}f'_{c}$ or $_{d}f'_{c}$ on the impulsive ultimate flexural capacity is more significant with the pre-tensioned type than the post-tensioned type.

(5) Comparison of Static Ultimate Flexural Capacity and Impulsive Ultimate Flexural Capacity

Figure 27 illustrates a comparison of the static ultimate flexural capacity S and impulsive ultimate flexural capacities (I_1 and I_2) in terms of positive rail-seat section flexure for typical JR sleepers (Fig. 2). Figure 27 also shows the evaluated result of ultimate sleeper flexural

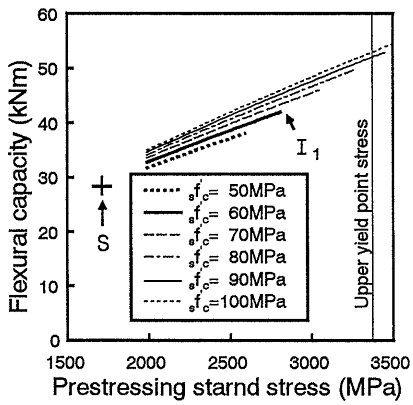

(a) Pre–tensioned 3PR type sleeper

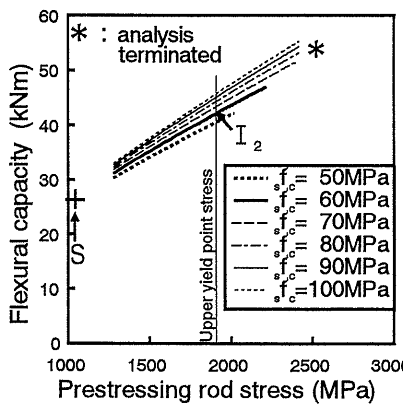

(b) Post–tensioned 3PO type sleeper(bonded)

Fig.26 Evaluation of impulsive ultimate flexual capacity (positive rail-seat capacity) moment obtained by Equation 2, with the maximum impact wheel load set to 400 kN. The diagram in Fig. 27 offers the following understanding:

1) When comparing pre-tensioned and post-tensioned sleepers of the same grade, both the static ultimate flexural capacity and impulsive ultimate flexural capacity of the post-tensioned sleepers were in general slightly smaller than those of the pre-tensioned sleepers. It should be noted however that these results were obtained assuming bonded prestressing rods in the post-tensioned sleepers. In the case of an unbonded configuration, the difference may be larger.

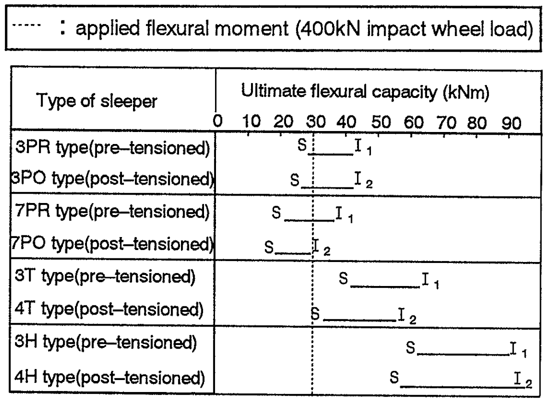

Fig.27 Evaluation of ultimate flexual capacities (positive rail-seat capacity)

2) The static and impulsive ultimate flexural capacities of PC sleepers designed by the conventional method significantly vary from one type of sleeper to another. Since the maximum impact wheel load can be considered not very different for wheel flat impacts in the lower speed range, the ultimate limit-state is essential, in addition to the serviceability and fatigue limit-states, as a factor for rationalizing PC sleeper design.

3) The effect of loading rate in strain on the upper yield point of prestressing steel is likely to be overestimated. It is therefore appropriate to interpret the impulsive ultimate flexural capacities discussed above as upper limits. Although, impulsive ultimate flexural capacity up to at least 140% of the static ultimate flexural capacity was experimentally verified with the 3PR type and 3PO type (unbonded), a more reliable study cannot be presented as yet. Accordingly, it is essential to be conservative in any safety evaluation for ultimate limit-state, introducing also an appropriate value of rupture safety factor.

10. PROPOSALS FOR LIMIT-STATE DESIGN METHOD OF PC SLEEPERS

A specific proposal for limit-state design is made below in terms of positive rail-seat flexure.

(1) Evaluation Method for Serviceability Limit-state

Since it is currently difficult to quantitatively evaluate cracking state on the basis of a cumulative frequency distribution curve of wheel load, we are obliged to experimentally or empirically assess the serviceability limit-state. When considering a severe loading environment, or planning the use of a new reinforcing material or new reinforcing system, it is desirable to conduct single-sleeper repetitive impact loading tests as discussed in 7. (1). In the case of mild loading environments, such as the current JR lines, the knowledge provided in 7 indicates that the following procedure may be suitable:

1) Pre-tensioned 3PR type sleepers exhibit, in single-sleeper repetitive impact loading tests, good cracking states under sleeper flexural moments induced by impact wheel loads up to 270 kN (wheel load impact factor $(1+i_d)=3.4$). The wheel load impact factor $(1+i_d)$ corresponding to the de-compression moment of the 3PR type sleeper, calculated by Equation 2, is about 1.5. Considering the fact that this type of sleeper exhibited a good cracking state under a moment up to 2.3 times as large as the de-compression moment, it can be said that the cracking control ability of pre-tensioned types is by far greater than conventionally predicted. Consequently, taking into account consistency with the generally excellent achievements of conventionally designed sleepers, the authors propose here, as a conservative design scheme for pre-tensioned types, determining the de-compression moment using Equation 2 with a wheel load impact factor $(1+i_d)$ of 1.5. However, judging from the good cracking states seen in the experiments, the factor can be reduced to about 1.0. For mild environments, wheel load impact factors from 1.5 to 1.0 are recommended for determing the de-compression moment as a serviceability limit-state design condition.

2) On the other hand, to restrict cracking to that of the serviceability limit-state, as mentioned in 7. (3) 4),

the de-compression moment of post-tensioned (unbonded) types should be at least 130% that of pre-tensioned types. In consequence, if the wheel load impact factor (1+id) is taken as 1.5 to 1.0 for pre-tensioned types, the de-compression moment of post-tensioned (unbonded) types should be evaluated using Equation 2 with a factor lying between 2.0 and 1.5, in the serviceability limit-state design for mild loading environments.

(2) Evaluation Method for Fatigue Limit-state

The fatigue lifetime as determined by prestressing steel rupture can be evaluated by the following procedure, based on the knowledge obtained in 8.

1) A cumulative frequency distribution curve of wheel loading is constructed, an example of which is shown in Fig. 28. It would be convenient to have a standard cumulative frequency distribution curve for wheel loads, constructed by means of systematic measurements and on the basis of factors such as wheel tread management conditions. Given that such a standard diagram is not available for the time being, it is vital to construct a temporary cumulative frequency distribution curve for wheel loads from engineering considerations, so as to achieve more rational sleeper design using the limit-state design method.

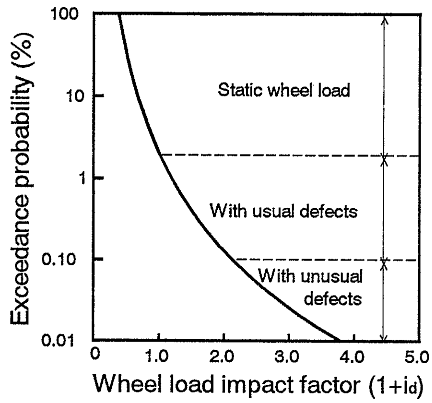

Fig.28 Cumulative frequency distribution curve of wheel loads (example)

2) The sleeper flexural moments are obtained by applying Equation 2 to the cumulative frequency distribution curve of wheel loads. The moments thus determined are converted by the computation method for PRC to a cumulative frequency distribution curve of prestressing steel stress.

3) The fatigue lifetime (service life) is evaluated by resorting to the cumulative frequency distribution curve of prestressing steel stress, the fatigue resistance of the prestressing steel, and Miner's hypothesis.

(3) Evaluation Method for Ultimate Limit-state

Sectional flexural failure can be studied by the following procedure, based on the knowledge obtained in 9.

1) As stated in 6. (2) b) 1), Equation 2 is likely to give a somewhat low value of sleeper flexural moment in the ultimate limit-state. What is practically more important is to determine a suitable maximum value of wheel load impact factor (1+id). As it is difficult at present to definitively specify an appropriate maximum wheel load impact factor (1+id), an approximate reference value of 5 is suggested here, as assessed from measurements currently available of maximum wheel load. Therefore, it seems satisfactory for the time being to implement sectional flexural failure studies using the moment obtained by Equation 2, taking (1+id) as 5.0.

2) With respect to sectional flexural failure, as discussed in 9. (5) 3), we are obliged to employ a conservative safety study method, using the impulsive ultimate flexural capacity obtained by the method explained in 9. (3) as the upper limit and an appropriate rupture safety factor. Nevertheless, such an approximate study of the ultimate limit-state will be help to avoid overdesign and underdesign, thereby contributing to rationalization of PC sleeper design.

3) If the impulsive ultimate flexural capacity of PC sleepers is evaluated with satisfactory accuracy, it will be possible to quantitatively study safety in terms of sectional flexural failure. To achieve this goal, the relationship between upper yield point of prestressing steel $d_{fy,u}$ and loading rate in strain $\dot{\varepsilon}$ should be quantitatively determined. This is the theme of a further investigation. Another subject of further investigation is to ascertain the lower impulsive ultimate flexural capacity of unbonded post-tensioned types as compared with bonded post-tension types.

11. CONCLUSIONS

A comprehensive study was implemented on the loading applied to PC sleepers, their structural response, and load carrying capacity, with a view to a shift from the conventional design technique involving "quasi-static load + static response + allowable stress" to a new design method factoring in "impact wheel load + dynamic response + limit-state behavior". The results of the investigations are summarized as follows:

1) Impact wheel loading can be modeled as a shock pulse acting for 1 to 10 msec. Its peak value, expressed by axle-box acceleration, reaches about 50g. Therefore, the impact wheel load may be 400kN or more, judging from the effective unsprung mass supported by each wheel.

2) By means of drop-weight impact tests and finite-element analysis, the influence of impulse duration on sleeper flexural moment was investigated. The study results revealed that positive rail-seat flexural moment reaches a dynamic loading peak about twice the static loading for an impulse duration of about 1.5 msec. This dynamic loading characteristic is due to the increased stiffness of the rail pad under the effect of loading rate in strain, coupled with the sleeper response resonance in connection with the impulse duration. A similar characteristic is also found for the negative flexural moment at the mid-span. The center-portion-free condition has almost no effect in the case of impact wheel loading acting for shorter duration than some 3 msec.

3) The relationship between sleeper flexural moment and impact wheel load was determined experimentally and analytically. Based on the results, a new design line (for the rail-seat section) and a new design line×2 (for the mid-span section) are presented in the form of dimensionless equations of design static wheel load P_{st} ; that is, Equation 2 (positive rail-seat flexural moment for narrow and standard gauges), Equation 3 (negative center flexural moment for narrow gauge), and Equation 4 (negative center flexural moment for standard gauge). The use of these equations was proposed for evaluating sleeper flexural moments in limit-state design. Moreover, through evaluating sleeper flexural moments in the ultimate limit-state using the equations proposed, and with the maximum impact wheel load set to 400 kN, it was found that the magnitude of flexural moment applied to the rail-seat section is about 3 and that to the mid-span section about 2, when taking the conventionally determined de-compression moments in the current design as unity.

4) The cracking state of sleepers was observed after 17,000 repetitions of single-sleeper impact loading. The test results revealed that the cracking state remains within the range allowable for the serviceability limit state when the flexural moment is up to 2.3 for the pre-tensioned type and 1.6 for the post-tensioned (unbonded) type, taking the conventionally determined de-compression moments in the current design as unity. This confirms that cracking control is better than the conventional prediction for a partial prestressing scheme, especially in the pre-tensioned types. The authors propose that, to restrict cracking to an identical serviceability limit-state, the de-compression moment for post-tensioned (unbonded) types should be at least 130% that of pre-tensioned types.

5) A prediction technique for fatigue lifetime in terms of prestressing steel rupture due to impact wheel loading was presented. Using this technique, the fatigue lifetime of typical JR PC sleepers was evaluated. The results specifically revealed, both for pre-tensioned and post-tensioned (bonded) types, that fatigue lifetime varies greatly according to the prestressing steel amount and the prestress level introduced, and that prestressing steel fatigue due to impact wheel loading is likely to be an important limit-state governing design, considering also the required lifetime of PC sleepers which may reach several hundred million cycles.

6) The evaluation method for impulsive ultimate flexural capacity involving impact wheel loading was reviewed, and tentative calculations were implemented for typical JR PC sleepers. Through this study, the impulsive ultimate flexural capacity was found to be given generally by I_1 (impulsive ultimate flexural capacity before upper yield point) for pre-tensioned types, and by I_2 (impulsive ultimate flexural capacity at upper yield point) for post-tensioned types. The authors specifically noted that the static and impulsive ultimate flexural capacities significantly vary by sleeper grade, and that, in addition to the serviceability and fatigue limit-states, the ultimate limit-state is also a primary consideration for achieving more rational design. To obtain accurate evaluations of impulsive ultimate flexural capacity, the relationship

between the upper yield point $\sigma_{fy,u}$ of the prestressing steel and the loading rate in strain $\dot{\varepsilon}$ should be quantitatively determined. This is a subject of further investigation.

7) Integrating the knowledge above, an outline proposal for a new design method combining "impact wheel load + dynamic response + limit-state behavior" was made. Instead of the conventional design, which is nominally based on a crack-free state with full prestressing, the new design method allows crack initiation and, provides designs that are more flexible but requires more extensive information, specifically corresponding to different loading environments and reinforcement means and materials. From a review of the pre-tensioned 3H type sleeper used for high-speed Shinkansen lines designed with the conventional full prestressing scheme, it was demonstrated that, even if the prestressing steel is reduced by 20% compared with the amount in the current design, this type of sleeper still has sufficient load carrying capacity to account for serviceability, fatigue, and ultimate limit-states. Cost optimization may be the greatest merit of the rationalized new design technique proposed here.

Ackowledgements

The authors gratefully acknowledge the guidance and help rendered by Dr. Shigeyoshi Nagataki, Tokyo Institute of Technology; Dr. Chitoshi Miki, Tokyo Institute of Technology; Dr. Kainen Watanabe, Kowa Kasei Co., Ltd.; Dr. Yoshihiko Sato, The Japan Mechanised Works and Maintenance of Way Co., Ltd.; Dr. Naohiko Miyata, Fuji P.S. Corporation; Mr. Koichi Shiina, Japan Railway Track Consultants Co., Ltd.; Mr. Iwao Iwasaki, Oriental Construction Co., Ltd.; Mr. Hisashi Asanuma, Kyokuto Kogen Co., Ltd.; and Mr. Hiromi Inoue, Railway Technical Research Institute.

References

[1] FIP Commission on Prefabrication: FIP State of the Art Report (Concrete Railway Sleepers), Thomas Telford Ltd., 1987

[2] Joint Committee on Relation between Track and Equipment AAR: Effect of Wheel Flats on Track and Equipment, AREA 53, 1952

[3] Y.Sato and M. Toyoda: Deformation of Tracks due to High-Speed Train Operation (Measurement Results of the Track Conditions on the Tokaido Shinkansen Model Line), Railway Technical Research Institute Report, No.492, August 1965 (in Japanese)

[4] ORE D 161.1 rp3: The Influence of Wheel Flats on Track with 20 and 22.5 t Axle Loads, Utrecht, September 1986

[5] F.E. Dean et al.: Investigation of the Effects of Tie Pad Stiffness on the Impact Loading of Concrete Ties in the Northeast Corridor, FRA/ORD-83/11, U.S. Department of Transportation

[6] H.P.J. Taylor: The Railway Sleeper (50 Years of Pre-tensioned Prestressed Concrete), The Structural Engineer, Vol. 71, No.16/17, pp.281-295, August 1993

[7] H. Wutzler: Spannbeton in den Gleisen der Deutschen Bundesbahn, Beton-und Stahlbetonbau 63, Ht. 5, pp.97-102, 1968.5

[8] Amir N. Hanna: Prestressed Concrete Ties for North American Railroads, PCI Journal, Vol. 24, No.5, pp.32-61, September-October, 1979

[9] I. Miura: Design and Manufacturing Methods of Prestressed Concrete Sleepers, Railway Technical Research Institute Report, No.307, May 1962 (in Japanese)

[10] Y.Sato: Cause of Severe Wheel Loads occurring with the Model 951 Test Car on the Tokaido Shinkansen Line and Countermeasures, Railway Technical Research Institute Report, No.824, September 1972 (in Japanese)

[11] I. Iwasaki and H. Asanuma: Performance Tests of Indented Prestressing Strands for Sleepers (Part 1), Railway Technical Research Institute Report, No.69-42, February 1969 (in Japanese)

[12] H. Wakui, H. Inoue, I. Iwasaki and H. Asanuma: Research on the Load Carrying Capacity of Aged Prestressed Concrete Sleepers, Summary of the 27th Conference of the Prestressed Concrete Engineering Association, pp.51-54, September 1987 (in Japanese)

[13] M. Miyamoto and I. Iwasaki: Static Flexural Capacity of Unbonded Prestressed Concrete Members, Railway Technical Research Institute Report, No.836, January 1973 (in Japanese)

[14] Y. Takahashi: Fundamental Study on the Impulsive Capacity of Reinforced Concrete Beams and Steel Plate-Concrete Composite Beams through High Speed Loading Tests, Doctorate Thesis (Kyushu University), December 1990 (in Japanese)